Chapter 6

Cosmic Ray Cradles in the Galaxy

Mehmet Guenduez, Julia Becker Tjus,
Björn Eichmann and Francis Halzen

Additional information is available at the end of the chapter

http://dx.doi.org/10.5772/intechopen.75429

Abstract

The search for the origin of high-energy cosmic rays has made significant progress in the past decade. By including multi-messenger methods, the general picture of the presence of a galactic component at low energies and an extragalactic one at the highest energies has been strengthened. Yet, unambiguous proof of the exact origins of cosmic rays is still missing. This chapter will review localized regions in the galaxy, which, due to their high nonthermal emission, are likely cosmic ray cradles. What we can learn from combining theoretical modeling with multi-messenger observations of regions like the Cygnus X complex, the Eta Carinae, and the Galactic Center region will be discussed. How the investigation of such localized regions in the Milky Way will help to resolve the more than 100-year-old question: *what is the origin of cosmic rays?* will be reviewed.

Keywords: cosmic rays, supernova remnants, Cygnus X complex, Galactic Center

1. Introduction

Galactic cosmic rays (GCRs) are defined as originating from outside our solar system but inside of the Milky Way. The cosmic ray (CR) spectrum in the range of ~ 10 GeV and 10^{15} eV and possibly beyond is believed to originate from the Milky Way. One of the main arguments for this hypothesis concerns the energy budget needed to produce the CR spectrum above ∼GeV energies, which cannot be reproduced by extragalactic sources but in particular by supernova remnants (SNRs) in the Milky Way [1]. The shock fronts of SNRs are well suited to accelerate charged particles via diffusive shock acceleration, which is another indication that SNRs work well as a particle accelerator. However, it is not clear yet how SNRs can reach the 10^{15} eV that is needed to reach the first kink in the CR spectrum, the so-called *cosmic ray knee*. Other sources like binary systems or pulsars could accelerate to even higher energies than

10^{15} eV. On the other hand, their total energy budget does not suffice to reproduce the intensity of the CR spectrum at Earth. In order to resolve the question of the origin of GCRs, nonthermal emission of photons and neutrinos can be investigated. Low-energy photons (in the radio to X-ray regime) comes from acceleration of electrons that suffer from synchrotron radiation and can thus be used to estimate the electron spectrum in dependence on the local magnetic field of the sources (see, e.g., [2] and references therein). High-energy photons can come from hadronic interactions via the production of neutral pions or leptonic processes like inverse Compton scattering or bremsstrahlung. This makes the interpretation of the signatures a challenge. The identification of galactic sources in neutrinos would help to identify the hadronic parts of the gamma spectrum, as neutrinos are co-produced with hadronic gamma rays via the decay of charged pions that are created in hadronic interactions. While a flux of astrophysical high-energy neutrinos has been detected for the first time in 2012 by IceCube [3], due to the low statistic of neutrinos, it is not resolved at the moment in which sources contribute to this diffuse flux. Thus, a combination of theoretical models with multi-messenger observations—also taking into account thermal and line emission signatures—is crucial to deduce information about the CRs and thus their formation process. It is advantageous to consider as much various measurements as possible to constrict the space of variation of the theoretical models. Once the various spectra and the ambient conditions from a potential CR object are known, we can constrict the source geometry, the radiating processes, and the properties of the attended CRs. In the next decades, as soon as we achieve the desired sensitivity for measuring neutrinos, the revelation of the origin of CRs is only a question of time. Theoretical predictions can lead the way to the first identification of the origin of GCRs. In this context, star-forming regions are crucial for the understanding of cosmic ray cradles, as all potential sources are correlated with star formation (or rather the dead of massive stars, which correlates with star formation). In this review, we therefore focus on recent results that could be achieved from the measurement and theoretical modeling of extended regions of CR emission and interaction. We will focus on the Cygnus region, the Galactic Center region, and the Eta Carinae region. In order to understand the connection between star formation and CRs, different correlations between wavelength bands can be investigated. In particular, such regions reveal a correlation between radio and far-infrared emission, as well as between radio and gamma-ray emission. In the introduction, we will review these correlations that are best established for starburst galaxies but exist locally in star-forming regions as well. Hereafter, Chapter 2 will focus on the general ansatz to describe CR transport and interaction in these extended regions. Chapter 3 will review the state of the art concerning measurements and modeling of the nonthermal emission regions Cygnus X, Eta Carinae, and Galactic Center.

1.1. FIR-radio, radio-gamma, and gamma-neutrino correlations

The first FIR-radio correlation was discovered in Seyfert galaxy nuclei by van der Kruit (1971). A general linear correlation for starburst galaxies was first discussed by Helou et al. [4]. Many attempts have been made to understand the proportionality between radio and far infrared. On the basis of rather simple modeling of galactic evolution, a strong correlation is actually expected, since both supernova remnants and the dominant heating by ultraviolet light from massive stars derive from the same stellar population [5, 6]. Using such models, the far-infrared

http://dx.doi.org/10.5772/intechopen.75429

luminosity of NGC2146 was predicted by [7], which is now observationally supported by IRAS observations [8]. The correlation as seen in the data was first clearly stated by [9] and subsequently discussed at some length by many authors; see, e.g., [10–12].

An extensive attempt to interpret the correlation was made by Völk and collaborators [13]. Here, the electrons lose all energy and therefore, the correlation is calorimetric. The model works quite well when considering the total energy budget, but it has some difficulties in explaining the observation of flat radio spectra also holding on small scales, which is not in concordance with the loss-dominated model. The solution of a spatial mixture of cutoffs would still allow for a locally loss-dominated scenario. Most recently, it was discussed that the nonthermal electrons that produce the synchrotron signatures are not those primarily co-accelerated with the hadrons but that they dominantly come from charged pion decays, which change the energetics of the problem [14].

Independent on the exact interpretation of the FIR-radio correlation, it indicates the coupling of particle acceleration (visible in the radio band) to star formation, seen via FIR emission.

The different formation processes and their connection are illustrated in the following **Figure 1**.

As the CR electrons also interact with the ambient photons and lose energy due to inverse Compton scattering, the FIR-radio correlation mainly depends on the average photon and magnetic field according to $q = 1 + U_R/U_B$ where $U_{R,B}$ denotes the averaged energy density of the magnetic field and photon field, respectively [13]. **Figure 2** demonstrates such a correlation.

1.1.1. Radio-gamma correlation

A correlation between radio and gamma emission has been found for a small number of objects that are detected by Fermi and that are expected to be dominated by signatures of star formation [16, 17]. Those objects that form the correlation are M 82, NGC 253, 1068, 4945, the Milky Way, and the Large Magellanic Cloud. Such a linear correlation is striking. First of all,

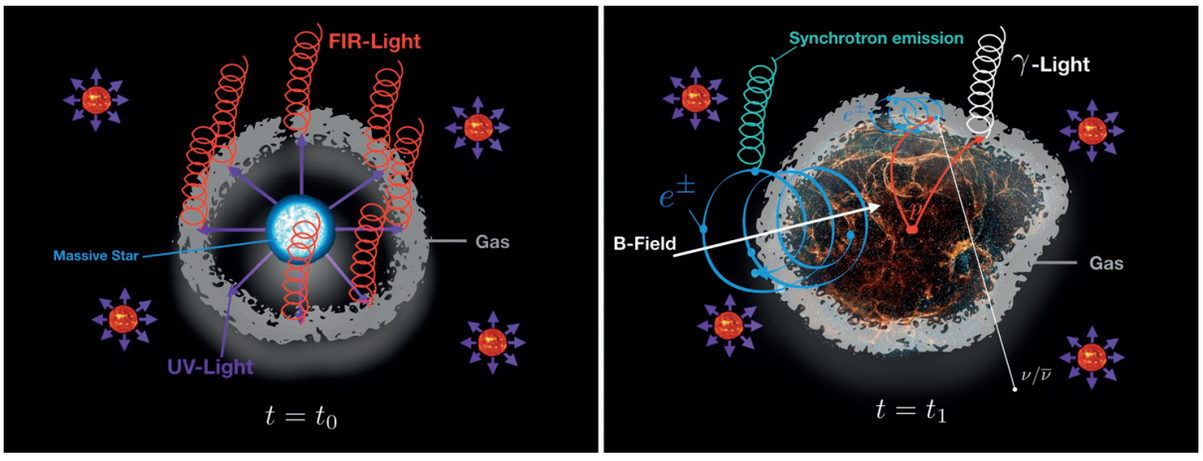

Figure 1. At $t = t_0$: A massive star emits UV radiation which is absorbed by the ambient gas; after that, it releases FIR radiation. At $t = t_1$: The massive star forms into a supernova remnant. The CRs from the SNR interact with the ambient medium and fields. As a result, γ-rays, neutrinos, and synchrotron radiation are produced.

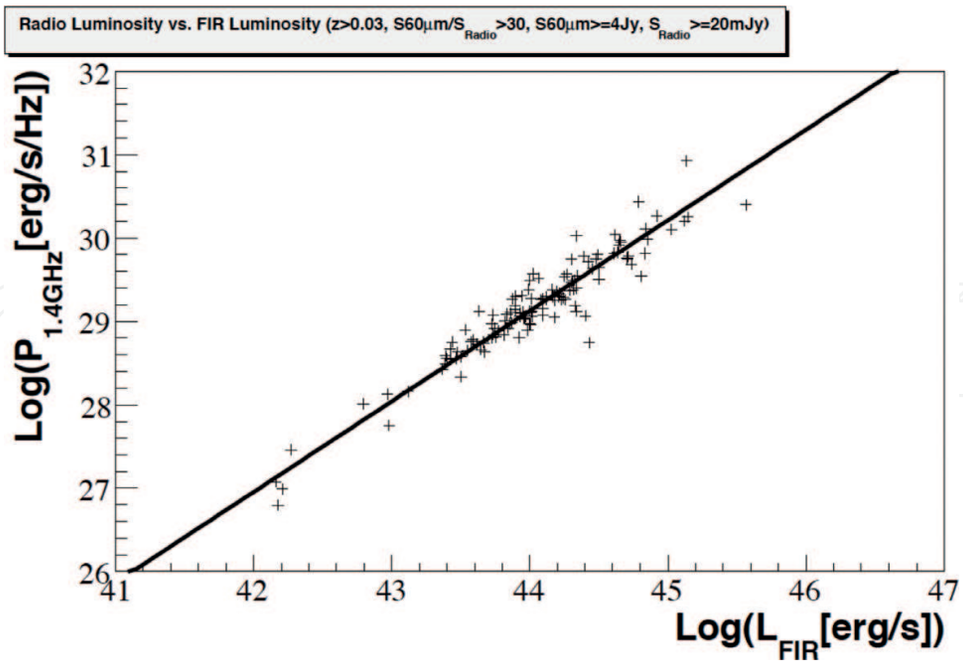

Figure 2. Correlation of L_{FIR} and $L_{\mathrm{Radio,\,1.4GHz}}$. Data from [15].

these are all objects of different sizes and level of star-forming activity. Secondly, gamma-ray emission is expected to be produced via hadronic interactions. Thus, the intensity should scale with the density of the ambient medium. On the other hand, radio emission is due to synchrotron radiation and thus depends on the magnetic field strength. It is therefore not necessarily natural that a linear correlation is established. A correlation between gas density and magnetic field strength, as established for different systems, could account for such an effect. This correlation has been investigated in detail for starburst galaxies by [18, 19].

1.1.2. Gamma-neutrino correlation

A source that is dominated by hadronically produced gamma rays should correlate with the neutrino strength of a source. However, for most regions in the sky, it is not clear if the detected gamma rays are of hadronic or leptonic nature.

The relevance of each process has to be restricted by considering reasonable arguments such as measurements at different energy ranges or neutrino spectra that accompany the γ-ray production due to the hadronic pion production. CR protons generate γ-rays due to the interaction with the ambient gas and CR electrons due to the interaction with an ambient photon field (inverse Compton) and the electromagnetic field of the ambient nucleus (nonthermal bremsstrahlung). All these processes can be formulated stochastically as energy spectra which are included in the integrand formulations of a specific flux. For clarification, all relevant processes for γ production and useful correlations are illustrated in **Figure 3**. As CR electrons and protons from a unique source, they can be correlated according to a quasi-neutral plasma, or in our galaxy (see [20] for a discussion), the relation of nonthermal radio and γ-ray emission is

http://dx.doi.org/10.5772/intechopen.75429

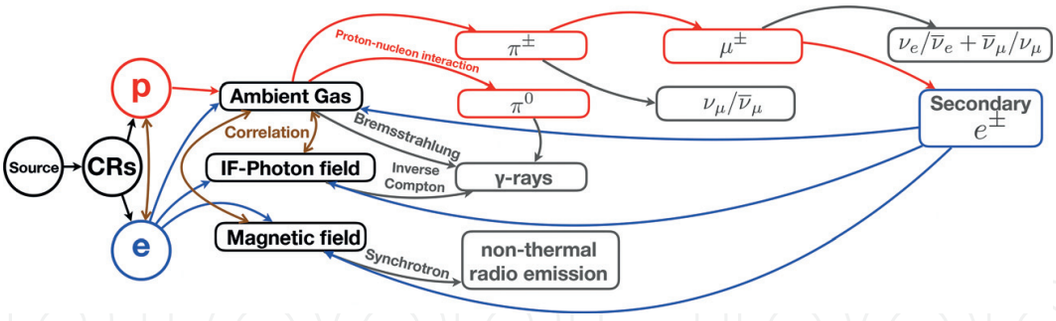

Figure 3. An illustration of the relation in star-forming regions and all relevant astrophysical processes in our galaxy: The red arrow represents the hadronic, the blue arrow the leptonic, and the gray arrow all processes which lead to the generation of radiations that can be measured and correlated. Lastly, the brown arrow illustrates the correlation of different physical quantities.

just a question of completeness of the considered processes which generate γ-rays and synchrotron radiation.

Thus, a gamma-neutrino correlation is based on all generation processes. Though neutrinos can be generated by CR protons, the consideration of leptonic processes is just as well important. Assuming that neutrinos are only produced in the processes illustrated in **Figure 3**, the γ-rays and neutrinos from the same source can easily be correlated. They can be correlated by considering the relevant energy spectra of neutrinos produced at proton-proton interaction following to [21] and by using the same normalization factor as for the γ-ray flux.

1.1.3. Conclusions for nonthermal emission from star-forming regions

In star-forming regions in the Milky Way, it has become obvious in the past decades through detections by Fermi, H.E.S.S., MAGIC, VERITAS, Milagro, and others that high energetic processes are omnipresent. The content of many massive stars leads to a high rate of a supernova explosion which releases high-energy CRs. On the one hand, the UV radiation of the massive stars collides with the high-density dust and generates FIR radiation. On the other hand, the released CR electrons are deflected by the ambient magnetic field which is related to the column density [22] and produce synchrotron radiation. Moreover, the released CR can cause γ-rays according to the processes in **Figure 3**. **Figure 3** illustrated all crucial relations and processes in star-forming region in our galaxy. Considering this relation, it is possible to correlate the FIR emission with synchrotron radiation as well as with γ-ray and neutrino emission. The procedure mentioned above is also illustrated in **Figure 1** (left) where the massive star at time $t = t_0$ sends out UV light that heats the ambient medium, which emits FIR radiation. **Figure 1** (right) exhibits the processes at $t = t_1$, after a supernova explosion, where synchrotron radiation dominates at low energies and hadronic emission together with IC and bremsstrahlung makes up the high-energy part of the energy spectrum.

Therefore, the star-forming regions such as starburst galaxies are natural laboratories for studying the FIR-radio and even radio-gamma or gamma-neutrino correlation as high-energy processes occur in these areas. Also, a correlation between the column density, IF photon field, and the magnetic field has been observed [22]. In total, γ-rays, synchrotron, and FIR emission

are reinforced by the high ambient gas density, amount of massive stars, and thus also SNRs. Due to their relation with CRs, the role of star-forming regions becomes of prime importance for the understanding of the origin and propagation of CRs.

2. Modeling nonthermal emission from star-forming regions

The dynamics in a star-forming region can be very complicated. It is therefore often necessary to work by simplifying assumptions which are reasonable and convenient to the relevant conditions. The ability to describe particle transport phenomena is indispensable for predicting processes in star-forming regions. The generic transport equation of the differential cosmic density $n(t, \mathbf{r}, \gamma)$ at a given time t, location $\vec{r}$, and particle Lorentz factor γ is given by [23]:

$$\underbrace{\frac{\partial n(\mathbf{r},\gamma,t)}{\partial t}}_{\text{Temporal Evolution}} \underbrace{-\nabla D(\mathbf{r},\gamma)\nabla n(\mathbf{r},\gamma,t)}_{\text{Spatial Diffusion}} \underbrace{-\frac{\partial}{\partial\gamma} b(\mathbf{r},\gamma) n(\mathbf{r},\gamma,t)}_{\text{Continuous Loss}} + \underbrace{\mathbf{v}\nabla n(\mathbf{r},\gamma,t)}_{\text{Advective Wind}} = \underbrace{Q(\mathbf{r},\gamma,t)}_{\text{CR Source Rate}} \tag{1}$$

Here, $\mathbf{v}$ is the advection velocity; in consideration, it represents the local wind structure that can be created through the density gradient which is present if a star-forming region of high density sits in a lower-density region of the galaxy. The diffusion tensor is denoted by $D(\mathbf{r}, \gamma)$, the continuous momentum loss by $b(\mathbf{r}, \gamma)$, and the source rate by $Q(\mathbf{r}, \gamma, t)$. Depending on the problem under investigation, the range of Eq. (1) can be extended by terms which consider a network of losses of the nuclei via spallation and by collision and decay.

Numerical approaches are helpful and are already performed for the investigation of our galaxy, e.g., by [24] or [25]. From the solution of the transport equation, Eq. (1), the differential cosmic ray density can be calculated. This can be done for hadrons and/or electrons, where different loss processes and source rates need to be considered depending on the species under investigation. The source rate can then be used to model the interaction with the ambient gas, magnetic field, or photon field. From the electron density, synchrotron radiation, inverse Compton emission, and nonthermal bremsstrahlung can be calculated. Focusing on high-energy hadronic processes (π^0, $\pi^{\pm}$, secondary $e^{\pm}$, ν; see red lines in **Figure 3**), the resulting fluxes Φ_{p_3} of the generated messenger particle of type p_3 at a distance d to the source are generally given by:

$$\begin{aligned}\Phi_{p_3}\left(E_{p_3}\right) = \frac{c}{4\pi \cdot d^2} \int_{r_{min}}^{r_{max}} \int_0^{\pi} \int_0^{2\pi} \int_{E_{p_3}}^{\infty} N_{p_2}\left(r,\phi,\Theta\right) n_{p_1}\left(E_{p_1}, r, \phi, \Theta\right) \\ \cdot \frac{\mathrm{d}\sigma_{p_1,p_2}\left(E_{p_1}\right)}{\mathrm{d}E} \cdot F_{p_3}\left(\frac{E_{p_3}}{E_{p_2}}, E_{p_1}\right) \frac{\mathrm{d}E_{p_1}}{E_{p_2}} \ \sin(\Theta)\ d\Theta\ \mathrm{d}\phi\ r^2\ \mathrm{d}r.\end{aligned} \tag{2}$$

Here, the specification is done by considering the cross sections σ_{p_1,p_2}, the energy spectra, F_{p_3}, e.g., from [21], and the reactant distribution N_{p_2}, where p_1 is an index that indicates the primary particle species (CRs, either protons or electrons) and the index p_2 relates to properties

http://dx.doi.org/10.5772/intechopen.75429

connected to the ambient reactant (photon field, magnetic field, or matter). Note that we suppose that all generated particles can escape free from the region of interest, i.e.:

$$1 \gg \tau_{p_1,p_2}\left(E_{p_1}\right) = \int_{r_{min}}^{r_{max}} \int_{f\left(E_{p_1}\right)}^{\infty} \sigma_{p_1,p_2}\left(E_{p_1}, E_{p_2}\right) \cdot n_{p_1}\left(E_{p_2}, r\right) \mathrm{d}r \, \mathrm{d}E_{p_2}, \tag{3}$$

with the minimum energy $f\left(E_{p_1}\right)$ of particle p_1 to interact inelastically with particle p_2. For the nonthermal Bremsstrahlung production, the flux simplifies and is given by:

$$\begin{aligned} \Phi_{\mathrm{BR}}\left(E_\gamma\right) = \frac{\left(m_p \cdot c\right)^{-1}}{4\pi \cdot d^2} \int_{r_{min}}^{r_{max}} \int_0^{\pi} \int_0^{2\pi} \int_{E_\gamma}^{\infty} N_t\left(r, \phi, \Theta\right) \frac{\sigma_{Br}}{E_\gamma} \\ \cdot n_e\left(E_e, r, \phi, \Theta\right) \mathrm{d}E_e \sin(\Theta) \; d\Theta \; \mathrm{d}\phi \; r^2 \; \mathrm{d}r \end{aligned} \tag{4}$$

with the bremsstrahlung cross section $\sigma_{Br} \simeq 3.38 \cdot 10^{-26}$ cm^2 and the proton target density N_t. The flux contributed by the inverse Compton (IC) process can be written as:

$$\begin{aligned} \Phi_{\mathrm{IC}}\left(E_\gamma\right) = \frac{3}{4} \frac{c \cdot \left(m_p \cdot c^2\right)}{4\pi \cdot d^2} \int_{r_{min}}^{r_{max}} \int_0^{\pi} \int_0^{2\pi} \int_{E_{min}}^{\infty} \int_0^{\infty} \frac{N_{IR}\left(\varepsilon, r, \phi, \Theta\right)}{\varepsilon} \\ \cdot \sigma_T \cdot n_e\left(E_e, r, \phi, \Theta\right) \frac{F\left(E_e, E_\gamma\right)}{E_e^2} \mathrm{d}E_e \, \mathrm{d}\varepsilon \sin(\Theta) \, d\Theta \; \mathrm{d}\phi \; r^2 \; \mathrm{d}r \end{aligned} \tag{5}$$

Here, σ_T denotes the Thomson cross section, N_{IR} the differential photon density, $F\left(E_e, E_\gamma\right)$ the Klein-Nishina related function, and $E_{min} = E_\gamma / \left(2m_e \cdot c^2\right) + \left(E_\gamma / (4\varepsilon)\right)^{1/2}$ the lower integration limit [26].

For the low-energy photon emission, the spectrum of synchrotron radiation can be derived by considering the total radiated power, which is performed isotropically; see [27] and references therein:

$$\begin{aligned} \Phi_{syn}(\nu) = \frac{P_0}{4\pi d^2} \left(\frac{\nu}{\nu_s}\right)^{1/3} \int_{r_{min}}^{r_{max}} \int_0^{\pi} \int_0^{2\pi} \int_{\gamma_{min}^e}^{\gamma_{max}^e} d\gamma \, \gamma^{-\frac{2}{3}} \\ \cdot n_e\left(\gamma, r, \phi, \Theta\right) \exp\left(-\frac{\nu}{\gamma^2 \nu_s}\right) \; \sin(\Theta) \; d\Theta \; \mathrm{d}\phi \; r^2 \; \mathrm{d}r, \end{aligned} \tag{6}$$

with $P_0 = 2.65 \cdot 10^{-10} \cdot \left(\frac{B}{1G}\right)$ eVs^{-1} Hz^{-1} and $\nu_s \simeq 4.2 \cdot 10^6 \left(\frac{B}{1G}\right)$ Hz as the characteristic frequency; see [18] and the references therein for the explicit mathematical derivation. While the above equations are in principle valid for an arbitrary region of cosmic ray emission, the adaption of the parameters in the equations, in particular the ambient conditions of the region of interest, is crucial to find a sufficiently accurate solution for the problem of consideration.

One simplifying approach to solve the transport equation, Eq. (1), is the consideration of a contained volume, the so-called leaky box model, where particles leak the volume due to diffusion and advection on the characteristic timescales τ_{diff} and τ_{adv}, respectively. Hence, the diffusion term can be replaced by $-n(\gamma, t)/\tau_{\mathrm{diff}}$ and the advection term by $n(\gamma, t)/\tau_{\mathrm{adv}}$. In doing

so, the solution just depends on the complexity of the source function and the continuous losses. Numerical approaches can treat the problem in a higher complexity; the analytical solutions have the advantage of being able to analyze the behavior of the source in more detail.

In the following, we will present three localized regions, which are star-forming regions and deserve an adapted formulation of the CR density.

3. Star-forming regions in the Milky Way and the nonthermal emission

3.1. Cygnus X

Cygnus X is a part of the largest star-forming region of the constellation Cygnus in the northern galactic plane and has a distance of 1.4 kpc from the Earth.

There are many reasons why Cygnus X is an excellent region to investigate the origin of CRs:

- The emission is observable from radio to high-energy gamma-ray frequencies [28], at which in the energy range from GeV up to TeV, Cygnus X has the brightest emission in the northern hemisphere [29].
- Many potential accelerators such as supernova remnants,[1] pulsars, and pulsar wind nebulae can be found. The Milagro detections at $>$ TeV energy point toward a possible hadronic emission scenario as leptonic processes cannot easily reach these energies, while they are natural for hadronic scenarios. IceCube has good visibility of the Cygnus region with muon neutrinos and could thus reveal a possible signal in neutrinos from that direction in the near future [31]. Many of these constituents are pictured in **Figure 4**.
- Cygnus X contains a large number of H $_{\text{II}}$ regions [32], indicating a high level of ionization —possibly caused by CRs; see, e.g., [33, 34].

All of these characteristics make Cygnus X a suitable natural laboratory for the astronomer to look beyond the usual constrained view.

The supernova remnant γ Cygni was first investigated using Fermi data, which provide information about the interstellar background by subtracting the radiation from γ Cygni. Cygnus X has a cocoon, in which freshly accelerated CRs are expected to be present, as its thermal emission exceeds 100 GeV. The SNR γ Cygni, which is in the cocoon, could cause the acceleration of protons even up to $80 - 300$ TeV and electrons up to $6 - 30$ TeV [35]. The accelerated particles could fill the whole cocoon if it is assumed that the main transport mechanism is diffusion [35]. Thus, γ Cygni has the potential to be the only accelerator in the cocoon. On the other hand, advection could dominate the transport mechanism, if an anisotropic emission of γ Cygni was observed [35]. Yet, there is still no final proof for this scenario. The cocoon could give hints about the transport mechanism and escape of CRs from their source.

[1] For example: γ Cygni J2021.0 + 4031e, which Milagro also detected at very high energies [30].

http://dx.doi.org/10.5772/intechopen.75429

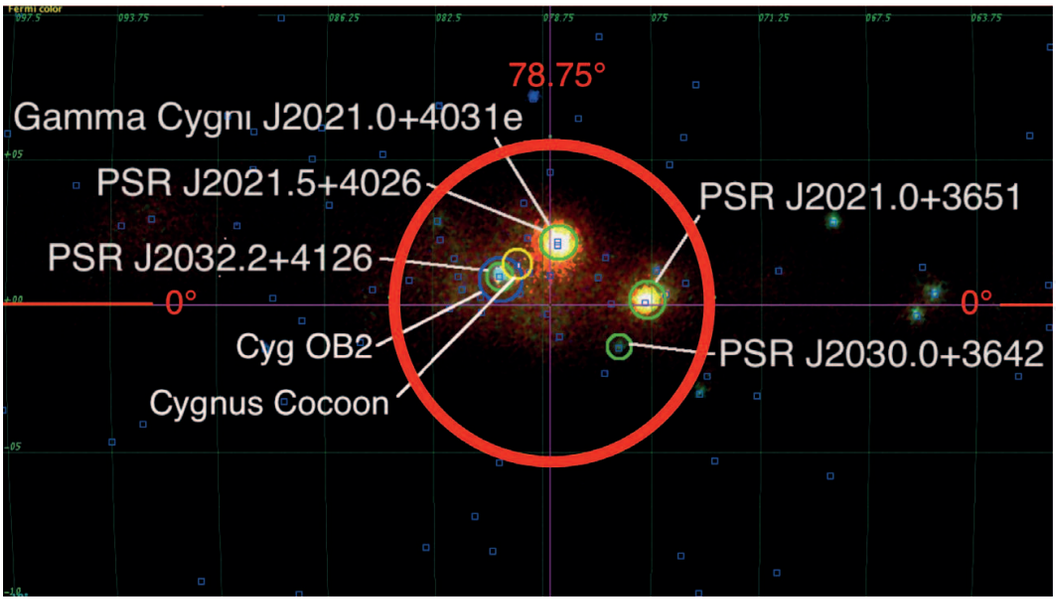

Figure 4. Fermi's color map of Cygnus X (red cycle) distributed by Skyview HEASARC—HEALPixed by CDS; the map was edited with Aladin v9.0. Additionally Cygnus X is pictured by a red cycle.

The modeling of the Cygnus region is based on the transport equation, Eq. (1). In order to solve the equation analytically, an emission from an isotropic and spatially homogeneous distributed part of the Cygnus region in its steady state is assumed. Additionally, a spatially independent diffusion of the particles within Cygnus X is applied. This assumption is reasonable since an extended region with a diameter of 77 pc will be considered, emission outside this zone is negligible, the region is very complex, and small inhomogeneities are expected to vanish at scales larger than the gyroradius. By this ansatz of the combination of a homogeneous injection and a leaky box, the variation of $n(\mathbf{r}, \gamma, t)$ only takes place at the scale of the radius of our region of interest. Using the quasi-neutrality of the plasma, the nonthermal radio and γ-ray emission can be correlated. This model has already been used for different starburst galaxies by [18], and details of the calculation can be found there.

As no accurate data about the ambient conditions are known, the spectral index α, the target density N_t, and the magnetic field B are kept as best-fit parameters which lead to a coincidence between nonthermal radio and γ-ray data and the prediction from the model.

The variated parameters as a function of χ are shown in **Figure 5**.

The continuous and catastrophic losses are essential for the transport within Cygnus X. **Figure 6** compares all relevant losses in Cygnus X for electrons and protons separately.

Hereafter, the different γ-ray and neutrino fluxes, which are caused by different processes as explained in **Figure 3**, can be calculated separately according to Eq. (2) and by considering the related CR density distribution in Eq. (1). The agreement between γ-ray, synchrotron emission, and the model can be seen by the following spectra.

The left spectrum of **Figure 7** displays the γ-ray flux considering leptonic as well as hadronic processes where the CR density has been derived for a homogeneous distribution in its steady

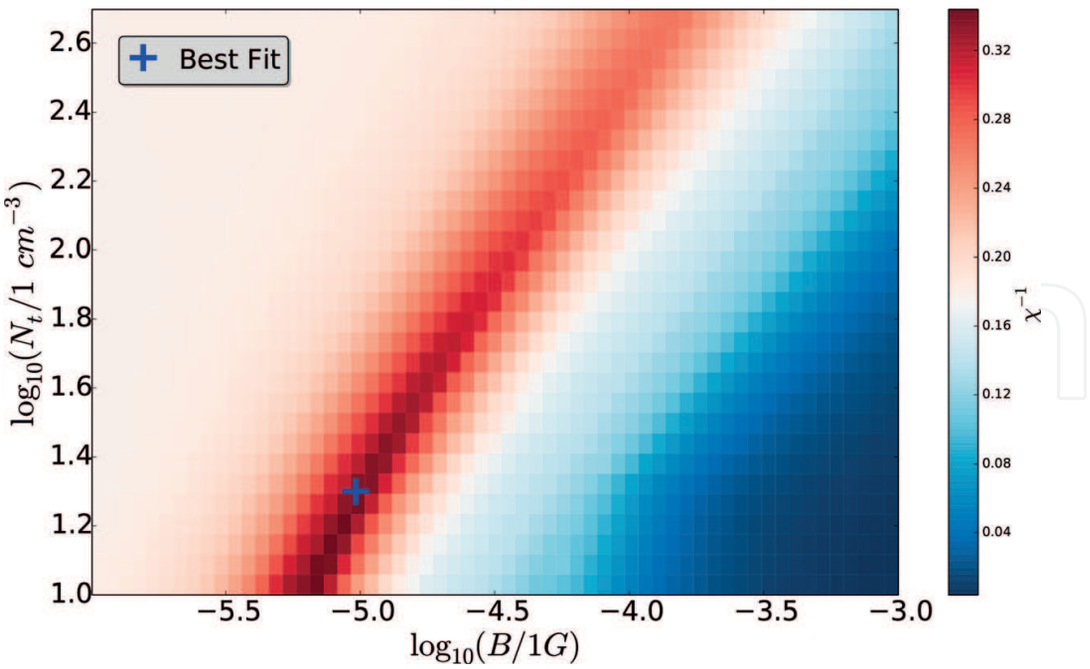

Figure 5. The total deviation χ^2 from the γ-ray and nonthermal radio data as a function of the magnetic field B and target density N_t. The best-fit parameters are represented by "+".

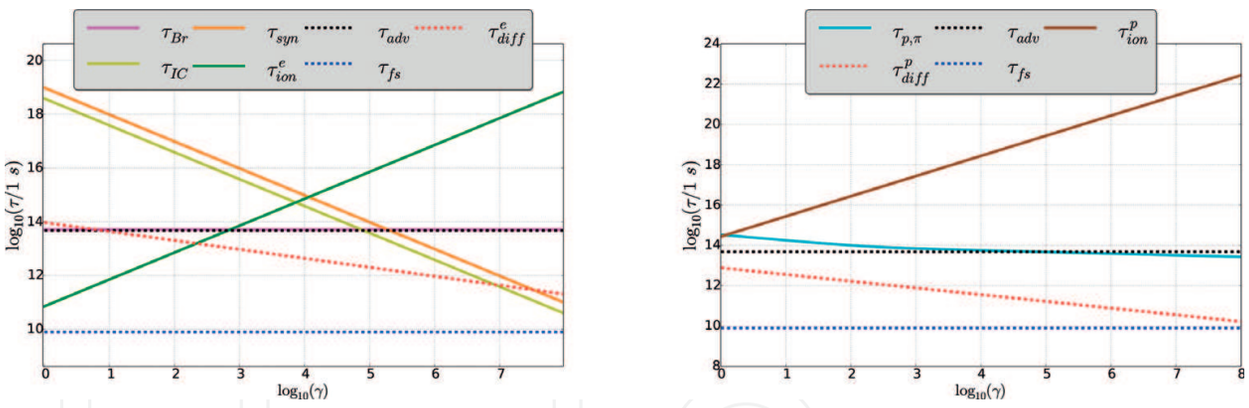

Figure 6. Continuous timescales (solid lines) and catastrophic timescales (dashed lines) for electrons (left) and protons (right) as a function of the Lorentz factor γ considering the best-fit parameters $\alpha = 2.4$, $N_t = 19.4\,\mathrm{cm}^{-3}$, and $B = 9 \times 10^{-6}\,\mathrm{G}$. Here, $\tau_{fs} = R/c$ denotes the timescale of a free-streaming particle with the velocity of light c.

state. Here, data from "Integral," "Fermi-LAT," and "ARGO-YBJ" as well as "Milagro" data, were considered. It is of great importance that data from "Integral" were taken into account, as the measurement at MeV energies strongly constraints the nonthermal bremsstrahlung and therefore the leptonic processes. Considering the synchrotron spectrum on the right side, a suitable diffusion coefficient helps to reach the γ-ray flux at 10 MeV and find the desired agreement.

The parameters from these spectra are used to find the neutrino spectrum which is displayed in **Figure 8**.

http://dx.doi.org/10.5772/intechopen.75429

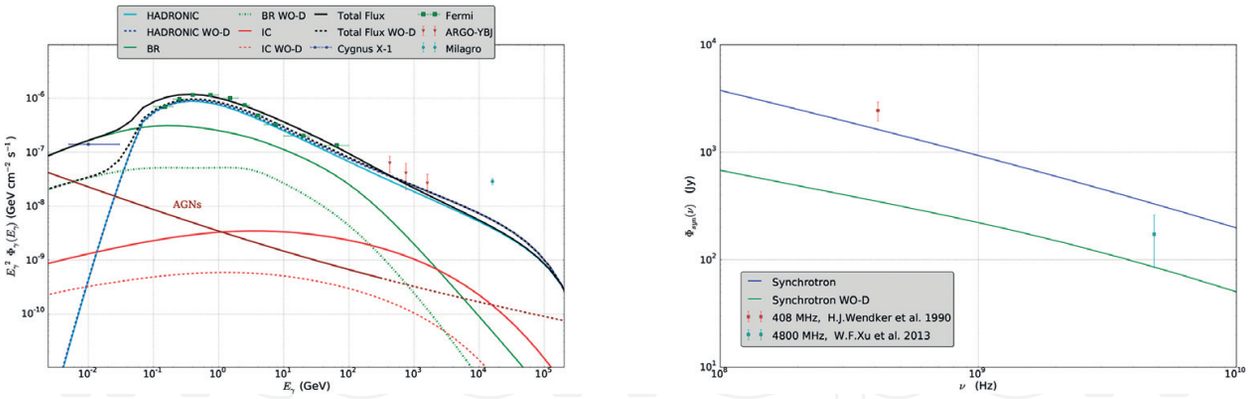

Figure 7. Synchrotron and γ-ray energy spectrum with and without (WO-D) consideration of diffusion; the source rate normalization factor q_0 was fitted on the observed gamma data.

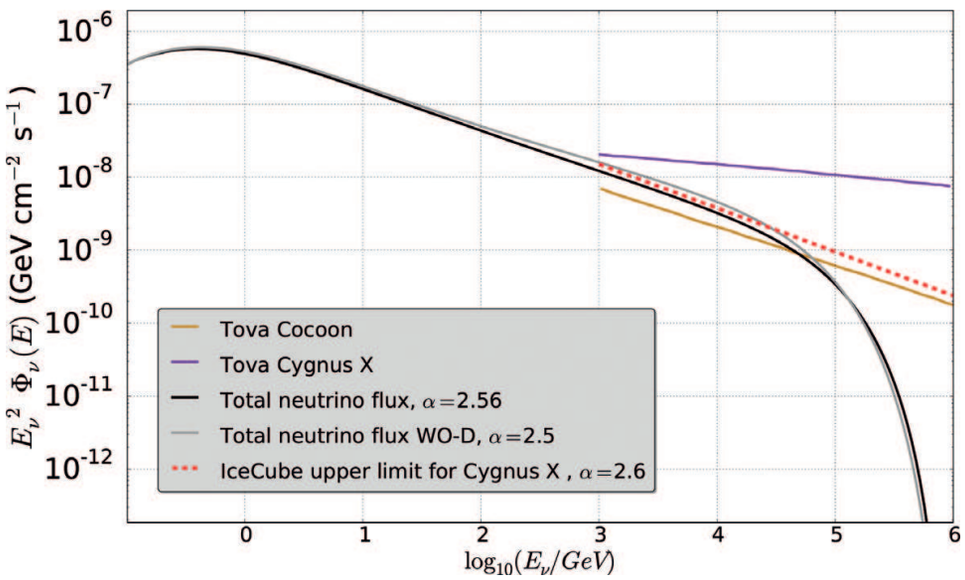

Figure 8. Differential neutrino flux considering new parameters with and without (WO-D) diffusion. A neutrino flux from an alternative model calculated by [36] and IceCube's upper limit calculated for Cygnus X [31] is also displayed.

The influence of the models is evident as Tova et al. [36] suggest a neutrino spectrum from Cygnus X which is most likely not detectable, whereas the model from this work coincides with the limit of IceCube. Additionally, in **Figure 8** the neutrino spectrum from Cygnus Cocoon is displayed, which has relatively a high flux. As IceCube has the highest sensitivity at 100 TeV and the spectral index of the predicted flux and the limit does not differ much from each other, a significant measurement by IceCube or IceCube-Gen2 may be soon possible. In fact, IceCube received already a 2 σ detection from Cygnus X. However, it is still not significant.

Tova et al. (2017) investigated the γ-ray and neutrino spectrum from Cygnus X by assuming that the CR spectrum observed at Earth is also a representative for the Cygnus X. This contribution has been added by emission from the Cygnus Cocoon separately as well as from

identified and unidentified point sources. All calculations were carried out for 5 deg. × 5 deg. region which is subdivided in 0.25 deg. × 0.25 deg. In contrast to the multiwavelength model in this work, which considered the whole region as one source, and radio and hard γ-ray emission, [36] just calculated and considered γ-ray emission. Here, the validation is only a question of time and just depends on the measurement of IceCube.

3.2. Eta Carinae

η Carinae is a binary system which contains a massive LBV star and an O- or B-type companion star and is located 2.3 kpc from the Earth [37]. Astronomers have recognized it in the past in the 1840s and 1890s due to series of giant outbursts, which now formed into a nebula. The binary system itself is the most prominent source of one of the most active star-forming regions in the Milky Way.

In the astronomically near future, the system is expected to implode into a supernova. It has been already detected from hard X-rays to high-energy γ-rays. It was observed up to 300 GeV by Fermi-LAT during its full orbital period of 5.54 years [37] which is most commonly interpreted as a colliding wind binary. This binary creates a very strong terminal wind velocity of $\sim 500 - 700\,\mathrm{km\,s^{-1}}$ [38]. Thus, the acceleration might be performed at the shock fronts of the extensive wind collision. The interaction between the accelerated CRs and the stellar radiation fields, the magnetic fields, and the surrounding plasma leads to high-energy nonthermal emission due to nonthermal bremsstrahlung, inverse Compton emission, synchrotron radiation, and hadronic pion production [39]. This motivated the H.E.S.S. collaboration in 2012 to observe η Carinae between Fermi and H.E.S.S. energies as only then H.E.S.S. could measure this region of interest. The observations from 2014 to 2015 achieved a 13.6 σ pretrial measurement for the combined data set [40]. These observations indicate that $\eta-$ Carinae could be another cosmic ray cradle in our galaxy.

Roughly, η Carinae can be sectioned into two phases:

1. Periastron passage: from the largest distance between both stars up to the shortest distance
2. Apastron passage: from the shortest distance between both stars up to the largest distance

A fully hadronic interpretation has been presented in [41]. In order to calculate the secondary emission from photons and neutrinos, it has been assumed that a fraction of $\eta < 1$ of the colliding wind luminosity goes into CRs. The wind luminosity is determined by the sum of the kinetic luminosities of the mass loss of the two stellar objects, so that $L_{CR} \approx 1/2 \cdot \eta \cdot \sum_{i=1,2}\left(\dot{M}_i \cdot V_i^2\right)$, with M_i as the $i = 1\mathrm{st}, 2\mathrm{nd}$ companion, $\dot{M}_i$ as the mass loss, and V_i as the wind velocity of the two individual objects. The result of this calculation is shown in **Figure 9**. Here, the result for Eta Carinae is compared to other Wolf-Rayet star binary systems, which only have limits from Fermi observations. The neutrino fluxes are calculated by assuming a gamma-ray flux at the Fermi limit and are therefore also to be considered as upper limits to a possible neutrino flux from these heavy binary systems in the Milky Way. The expected emission of these point sources is at low energies for neutrino telescopes, which makes them difficult to detect with IceCube or KM3NeT. An interesting opportunity in the future could be

http://dx.doi.org/10.5772/intechopen.75429

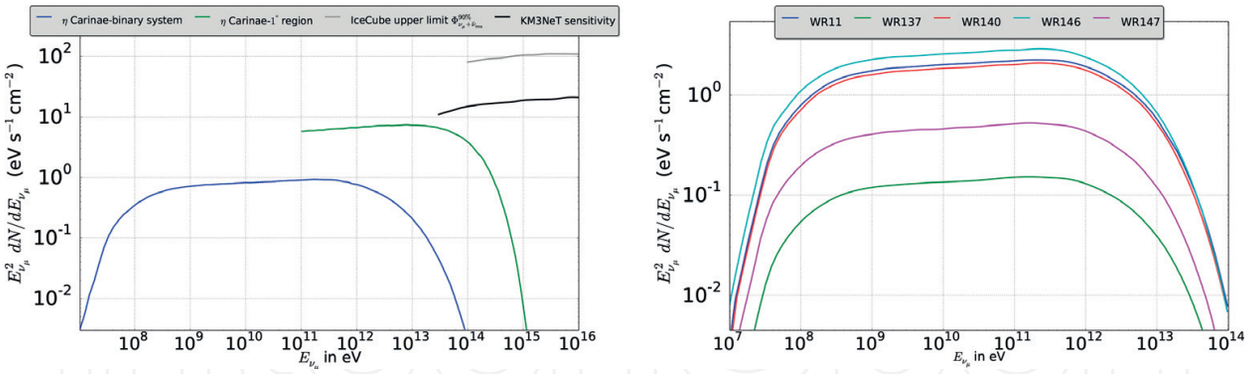

Figure 9. Left figure: neutrino energy spectrum of η Carinae during the 500-day periastron passage from [42] is shown in green, the neutrino spectrum of the binary system η Carinae calculated by [41] in blue, the IceCube upper limit in gray, and the KM3NeT sensitivity for the whole region of 1°. Right figure: neutrino spectrum of different Wolf-Rayet star binary systems.

searches for GeV neutrino sources with PINGU or ORCA. These have effective areas optimized to the GeV range, where atmospheric neutrino oscillations can be studied. At ~ 25 GeV, there is a minimum at which muon neutrinos from the atmosphere are strongly suppressed. This could open a small window in which the sensitivity for galactic GeV sources could be enhanced due to a strongly reduced background of atmospheric neutrinos [41].

A lepto-hadronic model to explain the nonthermal emission from Eta Carinae as an extended region has been presented in [42]. The spectral energy for both the periastron and apastron passage was derived. In this model, the part in the energy spectrum below 100 GeV is explained by inverse Compton emission. A prediction of a synchrotron spectrum is made in the radio to X-ray range. At the highest energies, $E_\gamma > 100$ GeV, the spectrum is explained by a hadronic component, with a prediction of the detection potential for H.E.S.S. and CTA. Although the CRs have been described by just a simple power law without any cutoff, the calculation of the flux considered the loss timescale, the maximum energy, ambient conditions, and the source geometry.

Deriving parameters from the comparison of the expected flux, observation data, and gamma-neutrino correlation, the neutrino flux can be predicted. **Figure 9** compares the prediction of the neutrino spectrum of η Carinae as derived from [41] (blue line) with the one in [42] (green line).

Considering the position of η nebulae and the size of $\sim 1^\circ$, one obtains an upper flux limit of $E^2\Phi^{90\%}_{\nu_\mu+\bar{\nu}_\mu} \simeq 1 \cdot 10^{-7}\,\mathrm{GeV\,cm^{-2}\,s^{-1}}$ for an E^{-2} unbroken power law of IceCube considering the 7-year data [43] (gray line), as also indicated in **Figure 9**. There is a difference of nearly one order of magnitude which is rather unrealistic to measure. With Eta Carinae in the southern hemisphere, the region is quite difficult to see for IceCube. A future surface array in connection to an IceCube-Gen2 array could change this.

Because of its location, KM3NeT has a better sensitivity to the southern hemisphere. For a 500-day exposure, the number of expected μ-neutrino events at KM3NeT for η Carinae between

10 TeV and 1 PeV amounts to 18 and for the diffuse astrophysical event to 0.03 [42], which could become interesting in the near future with a fully constructed KM3NeT detector.

3.3. Galactic Center

At a distance of 8.5 kpc from the Earth, the prominent supermassive black hole SgrA * represents the center of our galaxy. This central region in the galaxy is peculiar, as it reveals a high molecular density but no strong enhancement in star formation—a phenomenon that is also observed for other centers of galaxies [44]. Thus, it can formally not be considered as a star-forming region. Nevertheless, this region shows enhanced nonthermal emission at a broad energy range, which makes it equally interesting as those star-forming regions in the galaxy that we discuss here. This is linked with the ambient conditions but as well as with the sources within the region. SgrA * is surrounded by a circumnuclear disk (CND) with $R \simeq 3$ pc and a total mass of $10^6 M_\odot$ [45]. SgrA West the "minispiral," respectively, is a thermal radio source with three spiral arms of molecular gas that surrounds SgrA *. In every respect, the Galactic Center is very crowded especially by the stellar population as well as by molecular, atomic, and ionized gas. These characteristics make it rich on red giant stars, massive stars, and hundreds of OB and Wolf-Rayet stars [46]. Some prominent SNRs can be found near the Galactic Center, among those the prominent SNR SgrA East. This SNR is just 2.5 pc far away from the Center, has an elliptical shell along the galactic plane, and is surrounded by ionized gas. A visualization is exemplified in **Figure 10**.

SgrA * is supposed to generate high-energy CRs [47]. In fact, a diffuse γ-ray up to several tens TeV has been observed by H.E.S.S. within a radius of approximately 200 pc around the Center. Considering just a radius of about 8 pc, a large-scale diffuse radio emission, the radio halo, of a

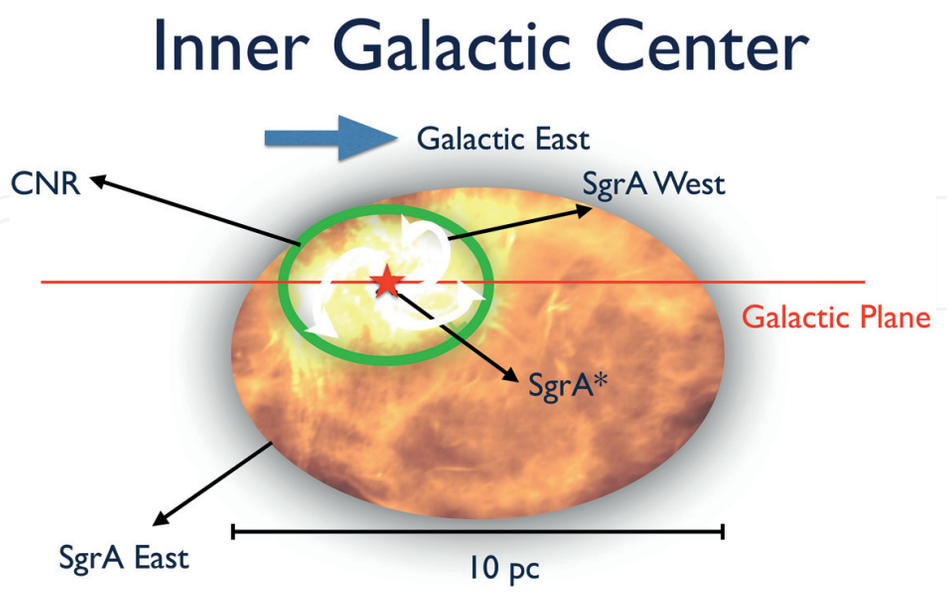

Figure 10. Inner 10 pc Galactic Center at 5 GHz.

synchrotron nature is present [48]. In contrast, a high-energy diffuse γ-ray emission contributed by electrons through the molecular zone is not realistic for various reasons:

- Electrons are susceptible to severe synchrotron and inverse Compton (IC) losses. Assuming a formation of high-energy electrons close to the black hole and a magnetic field strength of 100 μ G, the synchrotron timescale is $\tau_{\mathrm{syn}} \approx 7.7 \cdot \gamma^{-1}$ s, which corresponds to a mean free path of roughly $\lambda_{\mathrm{syn}} \approx 3.9 \cdot 10^{9} \gamma$ cm where γ denotes the Lorentz factor. Moreover, the ionization loss timescale yields $\tau_{\mathrm{io}} = 8 \cdot 10^{-10} \cdot \gamma \cdot \left(N_t / 5.7 \cdot 10^{4}\, cm^{-3}\right)$ s. In contrast, the diffusion timescale is given by $\tau_{\mathrm{diff}} = 2.1 \cdot 10^{8} \gamma^{1/3} \cdot (R/200pc)^{2} \cdot \left(D_0 / 4.7 \cdot 10^{27}\right)^{-1}$ s.
- The loss timescale inside the dense molecular clouds at the Galactic Center is much shorter than the propagation timescale. Thus, the γ-ray emission contributed by electrons is expected to be focused around a small region around the black hole.
- Therefore, a diffuse flux through the whole molecular zone demands an accelerator that boosts electrons up to $\geq$100 TeV [47] which requires unrealistic assumptions due to the diffusion and magnetic field.

Thus, the calculation of the diffuse γ-ray flux to describe the emission detected by H.E.S.S. [47] requires only proton transport Eq. (1). By maintaining the radial dependency, the γ-ray luminosity as a function of the distance from the center can be calculated. The measurement of this quantity has already been presented at H.E.S.S. energies ($E \geq 1$ TeV) by [47] and at Fermi (10 GeV $\leq E \leq$ 0.3 TeV) energies by [49]. [50] also take the radial dependency of the continuous momentum loss rate due to hadronic pion production and the target density into account. This consideration complicates the transport Eq. (1) but gives an insight into the source distribution and reveals the real origin of the diffuse γ-ray emission. In doing so and by considering an isotropic distribution of the CR injection and gas, [50] present a hadronic one-component model (1CM), which considers only SgrA * as the main source, and a two-component model (2CM) which considers SgrA * as well as the SNR SgrA East. **Figure 11** on the left side shows the calculated γ-ray emission from the hadronic pion production with the 1CM and 2CM. The filled blue circle is the measurement of Fermi-LAT PASS8 data [49] and the red filled triangles from H.E.S.S. [47]. The γ-ray fluxes in **Figure 11** denoted by "Gaggero 1 & 2" are calculated by [49] who consider the CR large-scale population and a hard and conventional diffusion. However, the flux denoted by "Gaggero 3" works with a best-fit procedure and does not consider CR large-scale population. Each of the calculations is based on extensive transport equation which is only numerically solvable and takes the general radial dependency and the radial component of the diffusion tensor into account [49].

The 2CM of [50] and the best-fit model of [49] describe the γ-ray data at higher energies sufficiently, though the best-fit model does not seem to consider a cutoff. Therefore, at higher energies, the discrepancies might become larger. The 2CM, which considers an exponential cutoff at 1 PeV, seems to describe Fermi-LAT as well as H.E.S.S. data best. However, only [50] tried to reproduce the γ-ray luminosity by their model. Due to the short distance of SgrA East to SgrA * ($\approx$ 2 pc), the radial distribution of the luminosity of both component models is quite similar and presented in **Figure 12**.

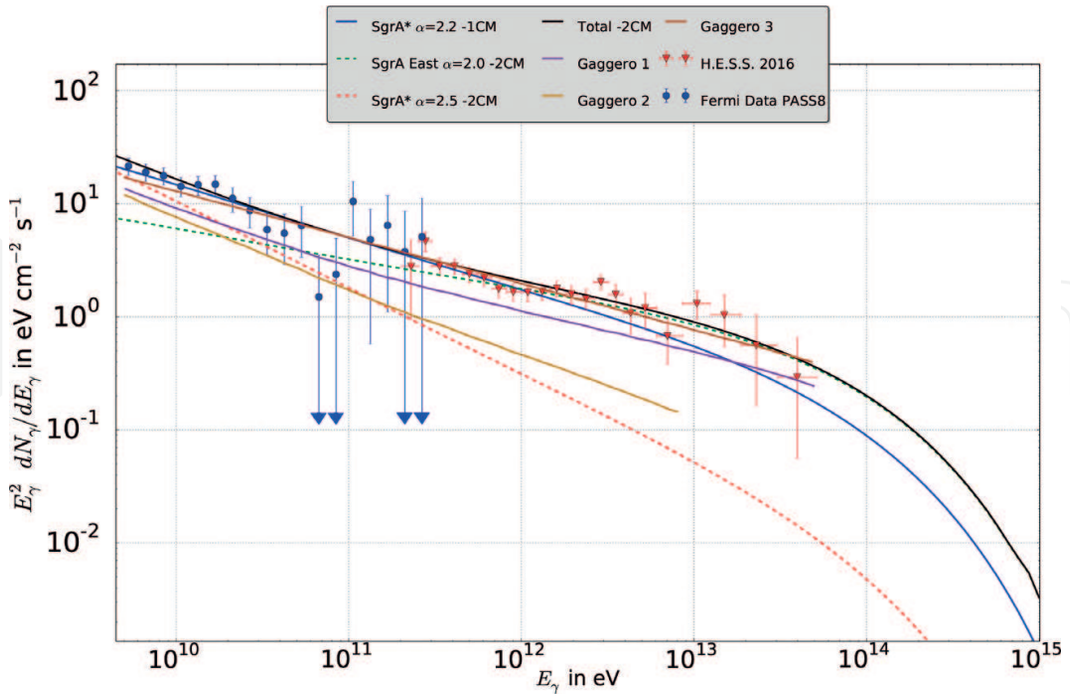

Figure 11. γ-ray emission from the inner 70 pc of the Galactic Center by [50] and by [49].

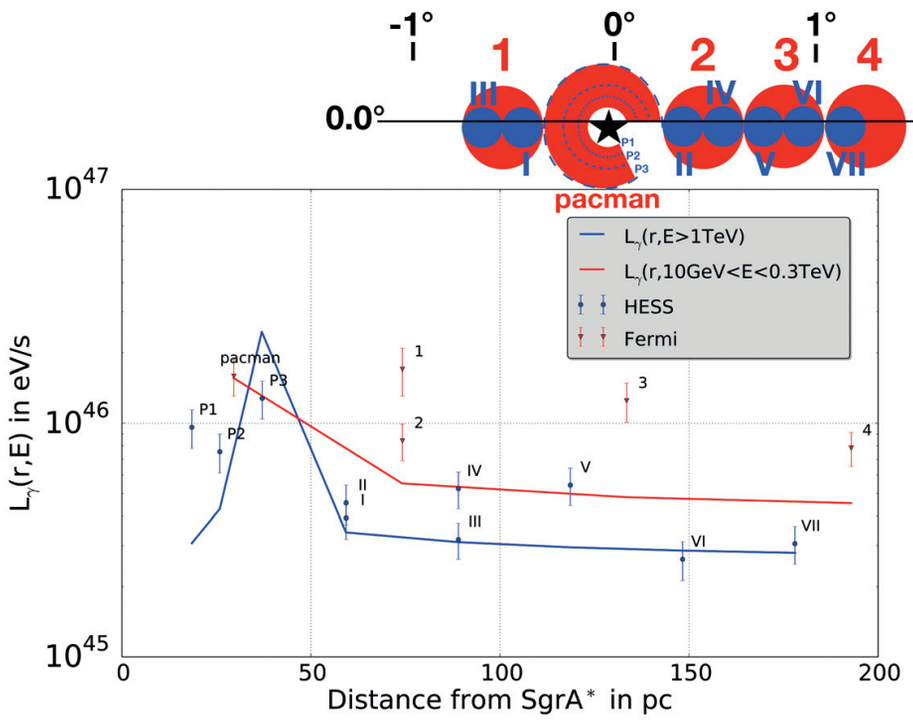

Figure 12. γ-ray luminosity as function of the distance from SgrA * for $E_{\text{cut}} = 1$ PeV.

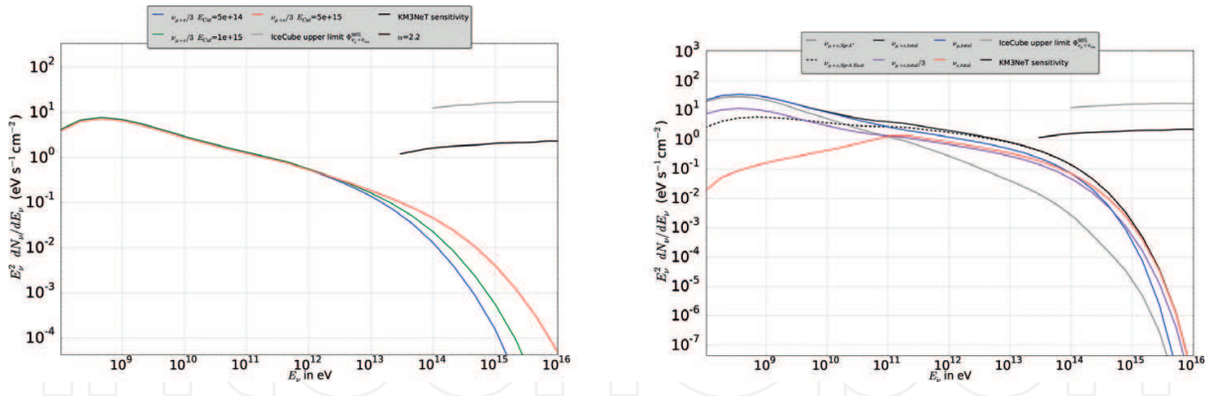

Figure 13. Neutrino spectrum from 1CM (left) and from 2CM (right) for $E_{\text{cut}} = 1$ PeV.

Although the radial distribution of H.E.S.S. is reproduced pretty well, the Fermi distribution exhibits discrepancies. This may be due to the simplification of the model which assumed an isotropic distribution around the Galactic Center or due to additional sources which are not identified or studied yet. The comparison between the expected and the measured luminosity does not suggest an isotropic injection of protons from one centrally located accelerator into the Central Molecular Zone as if it does it would not be able to suffice the observed luminosity. In contrast an additional source or sources could change the distribution in the right way. However, the model reproduces the γ-ray flux and the luminosity satisfactorily.

Accordingly, the neutrino spectrum is derived for the 1CM as well as for the 2CM.

Figure 13 also displays the IceCube's upper flux adapted for the region of interest as well as the sensitivity of KM3NeT. Again, due to atmospheric μ, the capability of KM3NeT is higher to detect neutrinos from the southern hemisphere and thus from the Galactic Center. Both observatories are still not able to detect any neutrinos from the direction of the Galactic Center.

4. Summary and outlook

Star-forming regions are of prime importance for investigating the origin of CRs, as they can be considered as CR birthplaces. During the past decades, a large variety of telescopes went into operation, starting to shed light on the nonthermal multi-messenger picture from star-forming regions in the Milky Way. Of particular interest are three concrete regions in the Milky Way:

1. *The Cygnus complex* is the most interesting star-forming region in the northern sky. It reveals nonthermal emission from diffuse regions and point sources up to $>$ TeV energy, in particular detected by the Milagro detector. This makes it a prime candidate to search for hadronic interaction signatures. The northern location is beneficial for the IceCube experiment, which can detect neutrinos in the TeV range with a spatial resolution of below 1° from the northern sky. The neutrino flux from Cygnus X approaches the IceCube's upper limit and past already the 2 σ deviations from background could be detected in the past. Model predictions show that a detection of the region could already be possible with IceCube, certainly with the next-generation array IceCube-Gen2 for a detection threshold in the TeV range.

2. The *Eta Carinae* region is of particular interest because of the binary system η Carinae, detected at energies from radio to gamma rays. It is one of the most energetic binary systems in the galaxy and could have the potential to accelerate hadrons at the shock front forming from the collision of the winds of the two massive stars. Gamma-ray fluxes for such binary systems are in general quite low, i.e., apart from η Carinae they are so far below the detection threshold of Fermi. Thus, even the expected neutrino flux is relatively low, with one more disadvantage of an energy cutoff at relatively low energy. A window of opportunity here could be the detection of astrophysical sources in the ~ 25 GeV neutrino energy range, as atmospheric muon neutrinos have an oscillation minimum here, which results in a highly reduced background.
3. The *Galactic Center* itself is no classical star-forming region, as—despite of the high molecular densities—the star formation rate is not increased in the amount expected for a correlation with the gas. It is, nevertheless, a region of high nonthermal emission. The most striking evidence for the existence of PeV CRs comes from H.E.S.S. measurements of the Galactic Center, where the gamma emission suggests a CR spectrum extending up to the knee. The question now is if a large part of the CR energy budget can come from that region or source or if this is a smaller part of the total energy budget. Neutrino measurements in the future by KM3NeT and IceCube-Gen2 will help to disentangle hadronic from leptonic signatures and thereby to quantify the hadronic contribution.

Future developments of telescopes will help to use star-forming regions in our galaxy in order to understand the birthplaces of CRs, i.e., the construction instruments like SKA, CTA, KM3NeT, IceCube-Gen2, and more. At least equally important is the proper modeling of these regions. Here, both plasma aspects, present in the transport equation via the diffusive and convective terms, and particle aspects, defined through the loss terms of leptons and hadrons, need to be considered in detail. Recent developments of numerical tools like CRPropa [25], DRAGON [51], GALPROP [52], and PICARD [53] represent important steps for a proper modeling, in which a diffusion tensor can be applied as well as hadronic and leptonic interactions with state-of-the-art cross sections that combine forward measurements with high-energy collision results at LHC. Thus, the next decade is very promising, as we will now be able to learn from this combination of precision astro- and astroparticle measurements and detailed theoretical modeling of the physics processes involved.

Author details

Mehmet Guenduez[1], Julia Becker Tjus[1]*, Björn Eichmann[1] and Francis Halzen[2]

*Address all correspondence to: julia.tjus@rub.de

1 Fakultät für Physik und Astronomie, RAPP Center, TP IV, Ruhr-Universität Bochum, Germany

2 Department of Physics, WIPAC, University of Wisconsin, Madison, WI, USA

References

[1] Becker Tjus J, Eichmann B, Kroll M, Nierstenhöfer N. Gamma-ray emitting supernova remnants as the origin of galactic cosmic rays? Astroparticle Physics. 2016;**81**:1-11

[2] Mandelartz M, Tjus JB. Prediction of the diffuse neutrino flux from cosmic ray interactions near supernova remnants. Astroparticle Physics. 2015;**65**:80-100

[3] Aartsen MG et al. Evidence for high-energy extraterrestrial neutrinos at the IceCube detector. Science. 2013;**342**:1242856

[4] Helou G, Soifer B, Rowan-Robinson M. Thermal infrared and nonthermal radio: Remarkable correlation in disks of galaxies. Astrophysical Journal Letters (United States). Nov 1985;**298**:2

[5] Biermann PL. On the radio continuum flux from the disks of spiral galaxies. Astronomy and Astrophysics. 1976;**53**:295

[6] Biermann PL, Fricke K. On the origin of the radio and optical radiation from Markarian galaxies. Astronomy and Astrophysics. 1977;**54**:461

[7] Kronberg PP, Biermann P, Schwab FR. The continuum radio structure of the nucleus of M82. The Astrophysical Journal. 1981;**246**:751

[8] Moshir M, Kopan G, et al. The faint source catalog, version 2.0. Bulletin of the American Astronomical Society. 1990;**22**:1325

[9] de Jong T et al. Radio continuum and far-infrared emission from spiral galaxies - A close correlation. Astronomy and Astrophysics. 1985;**147**:L6

[10] Wunderlich E, Klein U. A further study of the radio-far-infrared relation in galaxies. II—The ubiquity of the correlation. Astronomy and Astrophysics. 1988;**206**:47

[11] Wunderlich E, Klein U. The radio-far-infrared relation of interacting and non-interacting spiral galaxies. I - Observations and data collection. Astronomy & Astrophysics, Supplement Series. 1991;**87**:247

[12] Condon JJ et al. Correlations between the far-infrared, radio, and blue luminosities of spiral galaxies. The Astrophysical Journal. 1991;**376**:95x

[13] Völk HJ. The correlation between radio and far-infrared emission for disk galaxies - A calorimeter theory. Astronomy and Astrophysics. 1989;**218**:67

[14] Lacki BC, Beck R. The equipartition magnetic field formula in starburst galaxies: Accounting for pionic secondaries and strong energy losses. Monthly Notices of the Royal Astronomical Society. 2013;**430**:3171

[15] Becker JK, Biermann PL, Dreyer J, Kneiske TM. Cosmic rays VI—Starburst galaxies at multiwavelengths. ArXiv e-prints. Jan 2009

[16] Schöneberg S, Becker Tjus J, Schuppan F. A possible GeV-radio correlation for starburst galaxies. In: Torres DF, Reimer O, editors. Cosmic Rays in Star-Forming Environments. Vol. 34. Astrophysics and Space Science Proceedings. Springer; 2013. p. 299

[17] Becker JK, Schuppan F, Schöneberg S. A multifrequency view of starburst galaxies. Memorie della Societa Astronomica Italiana. 2012;**83**:154

[18] Eichmann B, Tjus JB. The radio-gamma correlation in starburst galaxies. The Astrophysical Journal. 2016;**821**:82

[19] Yoast-Hull TM, Gallagher JS III, Zweibel EG, Everett JE. Active galactic nuclei, neutrinos, and interacting cosmic rays in NGC 253 and NGC 1068. The Astrophysical Journal. Jan. 2014;**780**:137

[20] Merten L, Becker Tjus J, Eichmann B, Dettmar R-J. On the non-thermal electron-to-proton ratio at cosmic ray acceleration sites. Astroparticle Physics. Apr. 2017;**90**:75

[21] Kelner SR, Aharonian FA, Bugayov VV. Energy spectra of gamma-rays, electrons and neutrinos produced at proton-proton interactions in the very high energy regime. Physical Review D. 2006;**74**:034018

[22] Thompson TA, Quataert E, Waxman E, Murray N, Martin CL. Magnetic fields in starburst galaxies and the origin of the fir-radio correlation. The Astrophysical Journal. 2006;**645**(1): 186

[23] Ginzburg V, Syrovatskii S. The Origin of Cosmic Rays. 1st ed. Pergamon Press; 1964; p. 284

[24] Gaggero D et al. The gamma-ray and neutrino sky: A consistent picture of Fermi-LAT, Milagro and IceCube results. The Astrophysical Journal. 2015;**815**:L25

[25] Merten L, Becker Tjus J, Fichtner H, Eichmann B, Sigl G. CRPropa 3.1—A low energy extension based on stochastic differential equations. JCAP. 2017;**1706**(06):046

[26] Schlickeiser R. Cosmic Ray Astrophysics. 1st ed. Springer; 2002; p. 84

[27] Ghisellini G. Radiative Processes in High Energy Astrophysics. 1st ed. Springer; 2013; p. 43

[28] Virginia McSwain M, et al. Multiwavelength observations of gamma-ray binary candidates. Fermi Symposium proceedings—eConf C121028; 2012

[29] Abdo AA et al. Spectrum and morphology of the two brightest Milagro sources in the Cygnus region: MGRO J2019+37 and MGRO J2031+41. The Astrophysical Journal. 2012; **753**:159

[30] Abdo AA et al. Milagro observations of multi-TeV emission from galactic sources in the Fermi bright source list. The Astrophysical Journal. 2009;**700**:L127-L131

[31] Bernhard A. Origin of IceCubes astrophysical neutrinos: Autocorrelation, multi-point-source and time-structured searches [dissertation]. Technische Universität München; 2015

[32] Bartoli B et al. Identification of the TeV gamma-ray source ARGO J2031+4157 with the Cygnus cocoon. The Astrophysical Journal. 2014;**790**:152

[33] Becker JK, Black JH, Safarzadeh M, Schuppan F. Tracing the sources of cosmic rays with molecular ions. The Astrophysical Journal Letters. Oct. 2011;**739**:L43

[34] Schuppan F, Becker JK, Black JH, Casanova S. Cosmic-ray-induced ionization in molecular clouds adjacent to supernova remnants. Tracing the hadronic origin of GeV gamma radiation. Astronomy and Astrophysics. May 2012;**541**:317-324

[35] Tibaldoa L et al. The Fermi LAT view of Cygnus: A laboratory to understand cosmic-ray acceleration and transport. Nuclear Physics B, Proceedings Supplements. 2012;**230–240**:70-75

[36] Yoast-Hull TM, Gallagher JS III, Halzen F, Kheirandish A, Zweibel EG. The γ-ray puzzle in Cygnus X: Implications for high-energy neutrinos. Physics Review. 2017:**D96**(4):043011

[37] Reitberger K, Reimer A, Reimer O, Takahashi H. The first full orbit of η Carinae seen by Fermi. Astronomy and Astrophysics. 2015;**577**:A100

[38] Bednarek W, Pabich J. High-energy radiation from the massive binary system Eta Carinae. AAP. June 2011;**530**:A49

[39] Reimer A, Pohl M, Reimer O. Nonthermal high-energy emission from colliding winds of massive stars. The Astrophysical Journal. 2006;**644**(2):1118

[40] Leser E, Ohm S, Füßling M, de Naurois M, Egberts M, Bordas P, Klepser S, Reimer O, Reimer A, Hinton J. First results of Eta Car observations with H.E.S.S.II Proceedings of Science. 2017;ICRC2017:717

[41] Becker Tjus J. Neutrinos from colliding wind binaries: Future prospects for PINGU and ORCA. ASTRA Proceedings. May 2014;**1**:7

[42] Gupta N, Razzaque S. Lepto-hadronic model of gamma rays from Eta Carinae and prospects for neutrino telescopes. Physics Review. 2017;**D96**(12):123017

[43] Aartsen MG et al. All-sky search for time-integrated neutrino emission from astrophysical sources with 7 years of IceCube data. APJ. 2017;**835**(2):151

[44] Kennicutt RC, Evans NJ. Star formation in the Milky Way and nearby galaxies. ARAA. Sept. 2012;**50**:531-608

[45] Haardt F, Gorini V, Moschella U, Treves A, Colpi M. Astrophysical Black Holes. 2nd ed. Springer; p. 205

[46] Mauerhan JC, Cotera A, Dong H, Morris MR, Wang QD, Stolovy SR, Lang C. Isolated Wolf-Rayet stars and O supergiants in the Galactic Center region identified via Paschen-α excess. APJ. Dec. 2010;**725**:188-199

[47] Abramowski A et al. Acceleration of petaelectronvolt protons in the Galactic Centre. Nature. 2016;**531**:476

[48] Pedlar A, Anantharamaiah KR, Ekers RD, Goss WM, van Gorkom JH, Schwarz UJ, Zhao J-H. Radio studies of the Galactic Center. I—The Sagittarius A complex. APJ. July 1989; **342**:769-784

[49] Gaggero D, Grasso D, Marinelli A, Taoso M, Urbano A. Diffuse cosmic rays shining in the Galactic Center: A novel interpretation of H.E.S.S. and Fermi-LAT γ-ray data. Physical Review Letters. 2017;**119**(3):031101

[50] Guenduez M, Tjus JB. Modeling cosmic ray propagation in the Galactic Center region - Neutrino flux prediction and interpretation of the gamma-ray data from GeV to TeV energies. In preparation. 2018

[51] Evoli C, Gaggero D, Vittino A, Di Bernardo G, Di Mauro M, Ligorini A, Ullio P, Grasso D. Cosmic-ray propagation with *DRAGON*2: I. Numerical solver and astrophysical ingredients. JCAP. 2017;**1702**(02):015

[52] Moskalenko I. Modeling cosmic ray propagation and associated interstellar emissions. In: 39th COSPAR Scientific Assembly, Vol. 39 of COSPAR Meeting; July 2012. p. 1281

[53] Kissmann R. PICARD: A novel code for the Galactic Cosmic Ray propagation problem. Astroparticle Physics. 2014;**55**:37-50